Strain effects on the stability and structure of vacancy clusters in Si: A first-principles study

Robert J. Bondi, Sangheon Lee, and Gyeong S. Hwang*
Department of Chemical Engineering, University of Texas, Austin, Texas 78712, USA
(Received 26 January 2010; published 15 June 2010)

Using first-principles density-functional theory calculations, we investigate the influence of both biaxial and uniaxial strain ($-4\% \leq \varepsilon \leq 4\%$) on the stability and structure of small, neutral vacancy clusters (V_n, $n \leq 12$) on Si (100). A thorough understanding of vacancy clusters under strain is an important step toward elucidation of the evolutionary life cycle of native defects, especially during semiconductor manufacturing. Fourfold-coordinated (FC) structures are more favorable than "partial hexagonal ring" (PHR) structures in the size regime of our study under strain-free conditions; however, FC structures are also more rigid and consequently more sensitive to strain. Our calculation results indicate that PHR structures can be thermodynamically more favorable than FC structures in the presence of specific strain conditions. In addition, we identify orientation effects in which the cluster symmetry and its alignment within the strain field dictate cluster stability; in consequence, both configuration and orientation are essential factors in the identification of minimum-energy vacancy structures in strained Si. Furthermore, highlights of our simulation results suggest that minimum-energy cluster configurations formed under strain are often different than minimum-energy cluster configurations formed in the absence of strain.

DOI: 10.1103/PhysRevB.81.245206 PACS number(s): 61.72.jd

I. INTRODUCTION

Vacancies and interstitials are fundamental native defects that are ubiquitous to all crystalline materials and consequently of technological significance in semiconductor manufacturing because defects and impurities influence the electrical, optical, and mechanical properties of the host crystal. In particular, vacancies can be beneficial when adjacent to active electronic device regions by acting as gettering centers for impurities and through annihilation of self-interstitial defects; in contrast, vacancy clusters pinned inside active regions can be equally detrimental through impurity gettering and highly strained clusters can create deep-level traps that interfere with charge transport and degrade threshold voltages. During the production of crystalline silicon (c-Si), Czochralski-grown Si pulled from a liquid melt inherently contains grown-in vacancies and small voids.[1–3] High-energy irradiation using electron, neutron, and proton bombardment as well as mechanical plastic deformation can also introduce vacancies into Si.[4] In addition, many semiconductor manufacturing processes introduce vacancies including etching, thermal oxidation, thin-film deposition, and especially ion implantation.[5] Postimplantation annealing at elevated temperatures is further responsible for exacerbating vacancy agglomeration.

A variety of experimental techniques have been used to study vacancy clusters in Si, but a thorough understanding of vacancy behavior has thus far remained elusive. Positron annihilation spectroscopy is widely referenced,[1,4,6,7] but spectroscopic techniques, in general, cannot provide the structural configuration of small clusters. Transmission electron microscopy was used to substantiate the existence of small voids on the scale of a few nanometers,[8] but further resolution is needed to observe small clusters. In addition, fourfold-coordinated (FC) vacancy clusters are thought to be transparent to electrical methods such as deep-level transient spectroscopy and optical techniques such as photoluminescence.[6]

A complementary theoretical effort[2,4–7,9–15] has been made to support the experimental characterization of vacancies in Si. Many computational endeavors have sought to identify the minimum-energy configurations of small vacancy clusters, but most lacked a systematic method to search all complex, fully-coordinated configurations to determine the most favorable structures. Some early studies[5–7,10] focused on the ring hexavacancy (V_6) because of the exceptional stability suggested by its simple and complete FC configuration. Many of these same studies[5–7] concluded that partial hexagonal ring (PHR) configurations, which are formed by sequential removal of constituent Si ring atoms, would also represent the ground-state configurations of small vacancy clusters for $n < 6$, where n is the number of vacancies. Based on density-functional theory (DFT) calculations, Makhov and Lewis[4] proposed that small vacancy clusters (V_n, $3 \leq n \leq 5$) should favor complete fourfold coordination by nullifying all dangling bonds created by Si lattice atom removal via structural relaxation. The integrated atomic modeling procedure of Lee and Hwang[14–18] was recently extended to identify much larger, neutral FC configurations (V_n, $3 \leq n \leq 48$) and these studies indicate that FC structures are preferable to PHR-type configurations across this size regime.[14,15] Thus far, virtually all theoretical studies on vacancies in the literature focus on unstrained Si. A recent study[11] using kinetic Monte Carlo simulations investigates the anisotropic nature of vacancy behavior in uniaxially strained Si, but most conclusions concern vacancy-vacancy interactions rather than cluster formation and structure.

Strain engineering was widely embraced across the semiconductor industry in the 90 nm technology node as a cost-effective strategy to extend the electrical performance of digital complementary metal-oxide semiconductor transistors in accordance with Moore's Law.[19] There are two ways of technological significance to apply strain to the channel of a metal-oxide semiconductor field-effect transistor (MOSFET): (1) biaxial strain, which is sometimes referenced as global or bulk strain because it is implemented at

the substrate level and (2) uniaxial strain, which is sometimes identified as local or process-induced strain.[20]

In this paper, we investigate the effect of uniform strain fields on the stability, structure, and orientation of small, neutral Si vacancy clusters (V_n, $n \leq 12$) on both biaxially and uniaxially strained Si (100). Such small vacancy clusters on the subnanometer scale justify approximation of the applied strain fields to be effectively uniform in the immediate locale of the clusters. Our first-principles calculations simulate a bulk c-Si environment that might occur in the middle of a MOSFET transistor with a ⟨110⟩-aligned channel. The generation of all FC clusters studied was achieved using the integrated atomic modeling procedure of Lee and Hwang.[14–18] Our results provide an important step in the elucidation of vacancy behavior under strain, which is also essential to understand related native defect phenomena including vacancy agglomeration, self-interstitial annihilation, and stability near interfaces. Furthermore, our results highlight the influence of strain on the relative stability of FC and PHR-type clusters, the critical effect of cluster orientation on relative stability in anisotropic environments, and the propensity of strain to augment ground-state configurations.

II. COMPUTATIONAL DETAILS

All atomic configurations and energies reported herein were computed using a plane-wave pseudopotential method within the generalized gradient approximation of Perdew and Wang (GGA-PW91) (Ref. 21) to DFT (Ref. 22), as implemented in the Vienna *ab initio* simulation package (VASP) (Ref. 23). We employed Vanderbilt-type ultrasoft pseudopotentials[24] to represent electron wave functions. Valence-electron wave functions were expanded using a plane-wave basis set with a kinetic-energy cutoff of 160 eV. Brillouin-zone sampling was performed with one k point (at Γ) for optimization of atomic structures. Geometric optimization allowed all atoms to relax until residual forces between atoms had converged within 5×10^{-2} eV/Å tolerance. With optimized ionic positions determined, corresponding total-energy calculations were refined using a $2 \times 2 \times 2$ Monkhorst-Pack grid. For the strain-free Si supercell, we used an optimized lattice constant of 5.457 Å along ⟨100⟩ or 3.859 Å along ⟨110⟩.

To evaluate biaxial and uniaxial strain conditions, we computed a basis set of lattice vectors associated with a four-atom supercell for each strain condition ($-4\% \leq \varepsilon \leq 4\%$) and scaled the basis set up to each supercell size investigated. For this work, small clusters ($n \leq 3$) utilized 256-atom supercells, while all larger vacancy clusters used 480-atom supercells. For both basis supercells, we apply the same cell dimensions to the vacancy-containing supercells as calculated for the bulk Si reference supercells. Using this fixed-cell approach instead of a volume relaxation strategy is not only more representative of an isolated vacancy cluster in uniformly strained bulk Si, but also simplifies our calculations by allowing for a fixed set of dimensions to represent applied strain conditions for all cases of a given supercell size. Our preliminary calculations justified this fixed-cell approach in lieu of cluster-specific volume relaxation as long as the supercell chosen is sufficiently large for each cluster. For the smallest (largest) cluster studied in the 480-atom supercell, V_4 (V_{12}), we find volume relaxation to decrease the strain-free lattice constant by 0.2% (0.6%), while the strain-free formation energy decreases by 0.002 (0.05) eV per vacancy. While the percent change in lattice constant from volume relaxation is non-negligible for the largest clusters in terms of the applied strain conditions ($-4\% \leq \varepsilon \leq 4\%$), we maintain this will neither change the trends reported nor alter the conclusions of this study. To fully circumvent this size effect issue, supercells containing many thousands of atoms are required because the local strain fields generated by fourfold-coordinated clusters can be spatially extensive.

Since the effect of volume relaxation on strain-free vacancy clusters is larger on the lattice constants relative to the formation energies, we suggest that manifestation of this correction in formation energy as a function of strain throughout our reported results is largely a shift (left/right) of the formation energy curve on the order of ~0.1%. Volume relaxation on a vacancy cluster always reduces the supercell volume relative to bulk Si, so our formation energy curves as a function of strain will always shift to the right (slightly tensile), if this correction is applied. Sample calculations suggest that the correction magnitude obtained from volume relaxation tends to increase as the strain conditions become more compressive. Note that the relationship between lattice constant and applied strain is only one-to-one in the simple hydrostatic case; however, the relationship between a correction in lattice constant from volume relaxation and either a biaxial or uniaxial strain scenario is more complex. In fact, computing a formation-energy correction for biaxially or uniaxially strained vacancy clusters would necessarily depend on the supercell size (N), cluster size (n), and sign/magnitude of strain (ε).

As previously reported,[25–27] different cluster orientations also shift the qualifications of adequate supercell size to avoid periodic image effects. To circumvent the use of prohibitively large supercells, we equated the formation energies for all orientations at the strain-free condition to reference the lowest strain-free formation energy calculated. This same formation-energy correction was then applied to all strain conditions for a given vacancy configuration. This correction is only relevant in our results where multiple orientations converge to a single formation energy at the strain-free condition.

Figure 1 portrays the orientation of crystalline Si modeled with respect to both biaxial and uniaxial strain environments. To calculate modified lattice constants for strained Si systems, we quantified the Poisson effect depicted for both cases in Fig. 1. For the biaxial case, a quantity, ν^*, can be defined as the ratio of in-plane strain ($\varepsilon_\parallel$) and out-of-plane strain ($\varepsilon_\perp$). We compute the in-plane strain as $\varepsilon_\parallel = (a_\parallel - a_{Si})/a_{Si}$ and the out-of-plane strain as $\varepsilon_\perp = (a_\perp - a_{Si})/a_{Si}$. The values of $a_\parallel$ in our model system represent Si epitaxy grown over a binary SiGe alloy with lattice constant a_{SiGe}. The experimental value of a_{Si} is 5.4309 Å and a_{Ge} is 5.6461 Å (Ref. 28), so 4% tensile strain is the limiting case of Si grown over pure Ge. Using linear elastic theory[28–31] and published values[32] for elastic stiffness constants, we quantify the Poisson effect for the biaxial case as

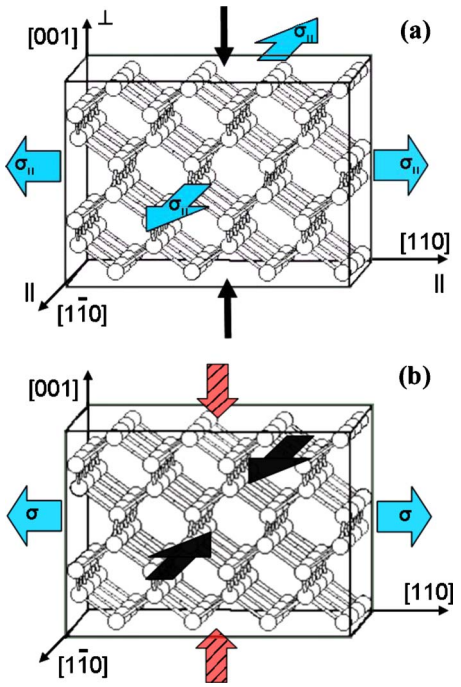

FIG. 1. (Color online) (a) Tensile biaxial stress/strain interaction in our model Si supercell. In the figure, applied tensile stress, $\sigma_{\parallel}$, in the plane of the substrate acts equally in all directions as shown by block arrows and produces a tensile strain. In response, the lattice contracts in the out-of-plane direction as shown by solid black arrows. For compressive conditions, the directions of all arrows are inverted. (b) Tensile uniaxial stress/strain interaction in our model Si supercell. For this case, tensile stress, σ, is independently applied along [110] and results in a corresponding strain along [110]. In response, the lattice dependently contracts along both [1$\bar{1}$0] (black arrows) and [001] (hatched red arrows). For compressive conditions, the directions of all arrows are inverted.

$$\nu^* = -\varepsilon_{\perp}/\varepsilon_{\parallel} = 2(C_{12}/C_{11}) = 0.771. \quad (1)$$

All results presented for biaxially strained Si use $\nu^*=0.771$ to calculate values of $a_{\perp}$ for each independent value of $a_{\parallel}$ investigated.

Similarly, the Poisson effect is used to quantify the strain relationships among different directions in the uniaxial case, but it is now necessary to determine Poisson ratios (ν) for two pairs of independent crystal directions because of the anisotropic nature of the crystal. We previously determined[27] these Poisson ratios and used them for the application of uniaxial strain to Si throughout this work,

$$\nu_{[110],[001]} = -\frac{\varepsilon_{[001]}}{\varepsilon_{[110]}} = 0.361, \quad (2)$$

$$\nu_{[110],[1\bar{1}0]} = -\frac{\varepsilon_{[1\bar{1}0]}}{\varepsilon_{[110]}} = 0.064. \quad (3)$$

With the Poisson ratios known and $\varepsilon_{[110]}$ independently defined by the sign and magnitude of strain imposed on the system, it is straightforward to compute uniaxially-modified values of $a_{[1\bar{1}0]}$ and $a_{[001]}$ for each independent value of $a_{[110]}$ studied. Perl scripts were generated to facilitate execution of numerous VASP simulations across the range of strain conditions studied.

Lee and Hwang[14] recently reported configurations of FC vacancy clusters (V_n, $3 \le n \le 18$) identified using an integrated atomic modeling procedure[14–18] combining Metropolis Monte Carlo (MMC), tight-binding molecular dynamics (TBMD), and DFT calculations. Figure 2 shows a subset of these same ground-state vacancy clusters (V_n, $3 \le n \le 12$) along with the fundamental monovacancy and divacancy clusters. These structures are the foundation for our strain investigation of vacancy clusters. As a consequence of the complex structure of many FC clusters, we have chosen to illustrate the clusters largely through identification of the highly strained atoms neighboring the vacant atoms, rather than representing vacant sites with visual identifiers that are often used to illustrate PHR-type clusters. Unless noted otherwise, a reference to V_n throughout this paper refers to the specific orientation and configuration of a cluster as shown in Fig. 2.

In our recent work,[25–27] we described the orientation-dependent stability for various interstitial cluster configurations on Si (100) under both uniaxial and biaxial strain conditions. For vacancy clusters in strained Si, cluster formation energies are also highly dependent on the cluster orientations with respect to the strain field. In concert with our previous work, we will adopt a similar orientation nomenclature as defined for interstitial clusters to present our results on vacancy clusters. The clusters shown in Fig. 2 represent the "A" orientation of each configuration; unless noted otherwise, a cluster without an explicit orientation label is the A orientation in Fig. 2. Note that the A orientation is essentially an arbitrary designation of the original cluster orientation. In special cases where we compare multiple clusters with identical symmetries, we have synchronized the orientation labels within the group to enhance clarity and facilitate discussion. The "B" orientation, which will only be studied under biaxial strain for our vacancy study, is formed by rotating a configuration in Fig. 2 so that an abstract axis aligned with [001] (out-of-plane) becomes aligned with either [100] or [010] (in-plane directions). The "C" orientation, which is only relevant for uniaxial strain in this study, is simply a 90° rotation of a configuration about an axis aligned with [001]. As depicted in Fig. 1, uniaxial strain is always applied along [110] throughout this paper. Further background on the orientation framework for clusters in crystalline Si was previously published.[27]

III. RESULTS AND DISCUSSION

To quantify the relative stability of Si vacancy clusters, we calculate formation energies dependent on both cluster size (n) and strain condition (ε) as follows:

$$E_f(n,\varepsilon) = E_{tot}(n,\varepsilon) - \frac{N-n}{N}E_{bulk}(\varepsilon), \quad (4)$$

where $E_{tot}(n,\varepsilon)$ is the total energy of the V_n cluster in the $N-n$ atom supercell, n is the size of the vacancy cluster, N is the basis number of atoms in the bulk Si supercell, and

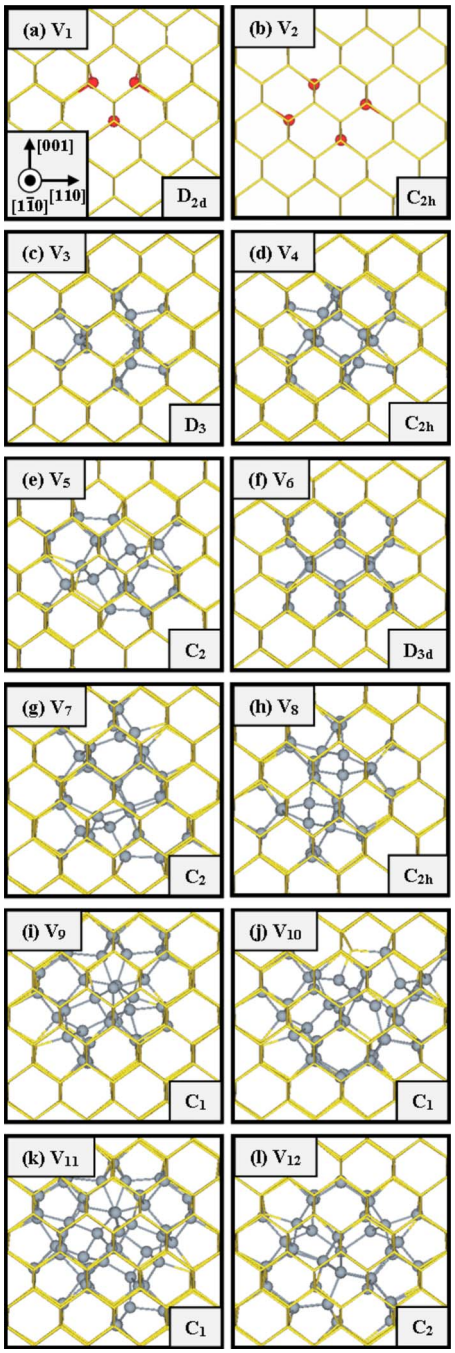

FIG. 2. (Color online) Strain-free, ground-state configurations of small, neutral vacancy clusters (V_n, $n \leq 12$) with corresponding cluster symmetries annotated. The perspectives shown for all clusters are defined to be the initial A orientations to facilitate discussion. Light gray (gold) wireframe represents bulk crystalline Si. Dark gray spheres represent highly strained atoms neighboring the vacancy clusters and red spheres represent atoms with dangling bonds. All structures are fourfold-coordinated except V_1 and V_2.

$E_{bulk}(\varepsilon)$ is the total energy of the N-atom supercell of crystalline Si at a given strain condition. We often report formation energies on a per vacancy basis; to ensure clarity in our results, we will label our formation energies using $E_f(n,\varepsilon) = n\hat{E}_f(n,\varepsilon)$, where $\hat{E}_f(n,\varepsilon)$ is formation energy on a per vacancy basis.

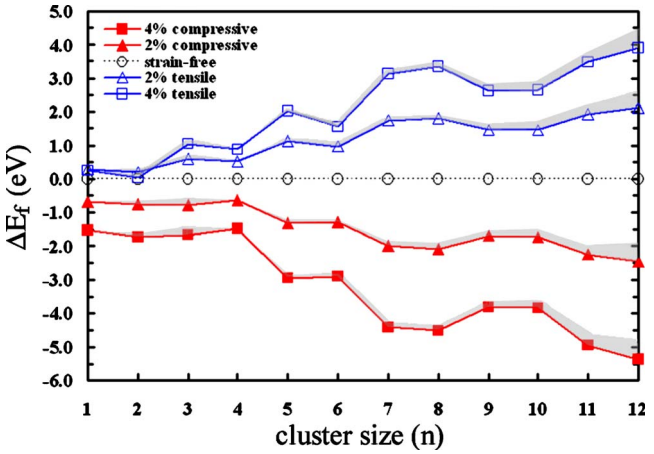

FIG. 3. (Color online) Formation-energy differences at discrete biaxial strain conditions for all ground-state vacancy-cluster orientations in Fig. 2 relative to their respective strain-free conditions. Compressive conditions are denoted by solid polygons (red). Tensile conditions are denoted by open polygons (blue). Gray shadowing added to each trend provides an approximate magnitude of adjustment that might occur if a correction based on volume relaxation is applied.

Figure 3 characterizes the general stability trend of the ground-state clusters of Fig. 2 under biaxial strain conditions. Unlike the trend previously published for interstitial clusters [see Fig. 5(a) in Ref. 25], Fig. 3 was generated by only evaluating the strain-free, minimum-energy configuration at each n for the orientations shown in Fig. 2. To emphasize this distinction, we provide formation-energy differences (ΔE_f) relative to the strain-free $E_f(n,\varepsilon)$ at various discrete strain conditions. In general, the formation energies tend to increase with increasing cluster size under increasingly tensile strain conditions, while the formation energies tend to decrease with increasing cluster size under increasingly compressive strain conditions. The variety of different configurations and cluster symmetries [Fig. 2] are considered largely responsible for abrupt cluster-to-cluster variations in $\Delta E_f(n,\varepsilon)$ as n increases. This cluster-to-cluster variation is not surprising since Lee and Hwang[14] show a similar nonmonotonic trend for $\hat{E}_f(n)$ for FC clusters under strain-free conditions. As expected, compressive strain tends to stabilize vacancy clusters, just as tensile strain was shown[25–27] to stabilize interstitial clusters. This result is intuitive since compressive strain tends to reduce the large interatomic distances for atoms neighboring voids in the crystal lattice.

To indicate how application of a formation-energy correction based on volume relaxation might adjust the trends in Fig. 3, a variable shadow has been drawn adjacent to each line based on sample volume relaxations of strain-free V_4 and V_{12} interpolated to other V_n and extrapolated to other strain conditions. The anticipated correction increases with n within each supercell size ($n \leq 3$, $N=256$; $n \geq 4$, $N=480$). The overall effect of the correction tends to shift all data in the tensile direction with respect to the strain-free reference because cluster-specific volume relaxation will compress each strain-free vacancy-containing supercell to some degree.

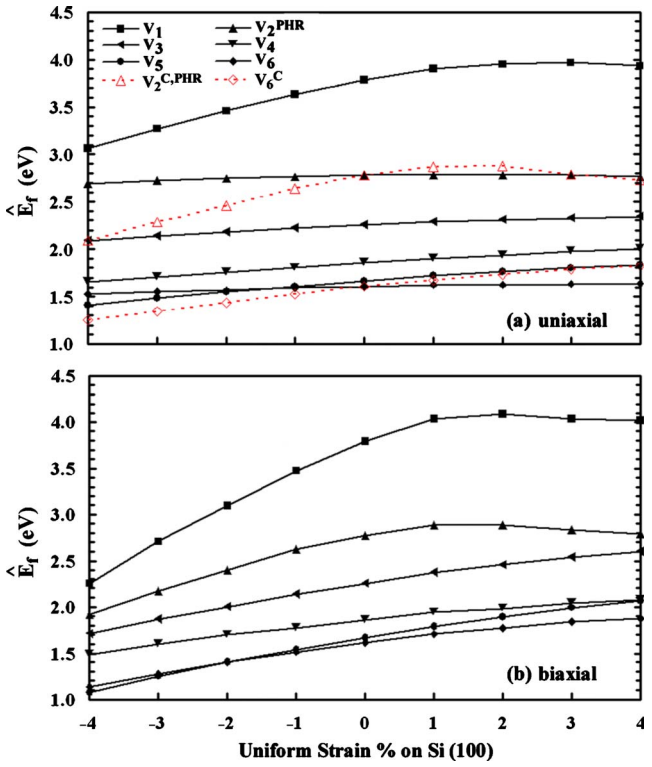

FIG. 4. (Color online) Formation energy per vacancy for the ground-state vacancy-cluster orientations in Fig. 2 (V_n, $n \leq 6$) as a function of (a) uniaxial strain and (b) biaxial strain. Tensile strain is defined to be positive. All configurations represented by solid (black) markers are in their initial A orientations, while the C orientations (only relevant for uniaxial strain) are represented by open (red) markers.

Figure 4 shows the formation-energy response curves as a function of strain for the minimum-energy configurations of V_1 through V_6. Since compression stabilizes vacancy clusters, the trends tend to have positive slopes, complementary to the negative slopes exhibited for interstitial clusters.[25–27] Consistent with our previous work on interstitial clusters, the $\hat{E}_f(n,\varepsilon)$ response (slope) is generally more sensitive to biaxial strain relative to uniaxial strain. A prominent feature, particularly in the biaxial case [Fig. 4(b)], is the flat $\hat{E}_f(n,\varepsilon)$ response under tensile conditions for both the monovacancy and divacancy. This behavior is similar to the general observation of flatness in the total energy as a function of ionic coordinate.[12,14] Our initial observation of the flatness of $\hat{E}_f(2,\varepsilon)$ for V_2^{PHR} [same configuration and orientation as V_2 in Fig. 2(b); PHR significance will be emphasized in Sec. III B] under uniaxial strain suggested a possible orientation effect like those previously described[25–27] for interstitials. This motivated further study and our inclusion of the C orientations for uniaxial strain of both V_2^{PHR} and V_6. Recall that the V_6 hexavacancy is a complete ring of vacancies in the Si lattice; while it exhibits strain-dependent behavior like PHR-type defects, it is also technically an FC structure. From Fig. 4(a), it is apparent that the A orientations of V_2 and V_6 are essentially insensitive to uniaxial strain, while the C orientations show more sensitivity to strain.

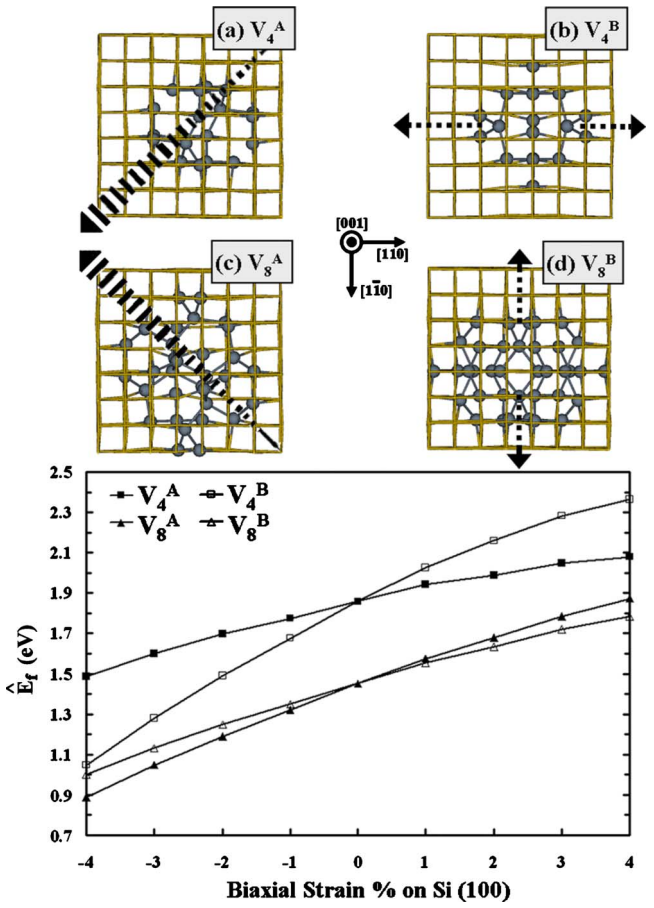

FIG. 5. (Color online) Formation energy per vacancy as a function of biaxial strain for the two relevant orientations of the C_{2h}-symmetry configurations of V_4 and V_8. The A orientations are depicted with solid polygons, while the B orientations are depicted by open polygons. The upper panel shows each orientation as viewed along [001] with corresponding C_2-symmetry axes indicated by black arrows. Light gray (gold) wireframe represents bulk crystalline Si. Dark gray spheres represent highly strained atoms neighboring the vacancy clusters. For the A orientations in (a) and (c), the C_2 axes trace a diagonal path through the supercell interior and emerge from the page at 45° angles, while the C_2 axes for (b) and (d) are contained in the plane of the page.

A. Orientation effects under biaxial strain

The phenomenon of orientation-dependent stability of interstitial clusters in uniform strain fields was a central feature in our previous work.[25–27] Due to the time-consuming nature of generating and investigating relevant cluster orientations, only selected V_n were investigated based on their group symmetry classifications.

Interstitial clusters with C_{2h} symmetry, such as I_{12} (Ref. 26), exhibit orientation-dependent behavior under biaxial strain. As a result, the C_{2h} configurations of V_4 [Fig. 2(d)] and V_8 [Fig. 2(h)] were likewise evaluated for a possible orientation effect. The B orientation counterparts of the Fig. 2 A orientations were generated. Figure 5 shows that V_4 and V_8 indeed exhibit orientation-dependent $\hat{E}_f(n,\varepsilon)$ behavior. As in the interstitial case, an orientation-dependent strain response corresponds to C_2-symmetry axis alignment relative

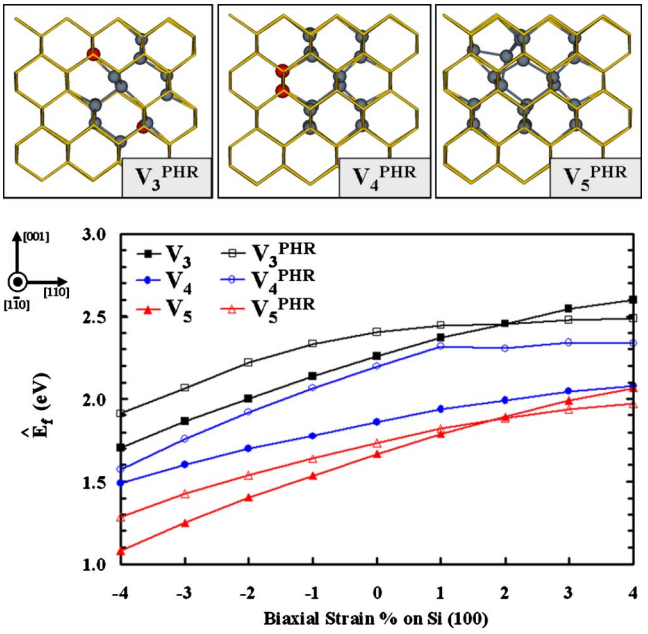

FIG. 6. (Color online) Formation energy per vacancy as a function of biaxial strain for both ground-state (solid markers) and PHR-type (open markers) configurations for $n=3-5$. The strain-free, ground-state FC structures are depicted in Fig. 2, while the upper panel shows the corresponding PHR-type configurations. Light gray (gold) wireframe represents bulk crystalline Si. Dark gray spheres represent highly strained atoms neighboring the vacancy clusters and red spheres represent atoms with dangling bonds.

to the plane of strain. Unlike the interstitial case, C_2-axis alignment with the plane of strain does not indicate how the sensitivity of $\hat{E}_f(n,\varepsilon)$ will change. For V_4^{B}, the slope of $\hat{E}_f(4,\varepsilon)$ increases relative to V_4^{A}, while the slope of $\hat{E}_f(8,\varepsilon)$ for V_8^{B} decreases relative to V_8^{A}.

B. PHR and FC relative stability

An array of literature exists on the structure and stability of small vacancy clusters in Si. In particular, the work of Lee and Hwang[14] showed that FC vacancy clusters are thermodynamically favored over their PHR counterparts over the entire size range $n=3-18$. While this observation holds in the strain-free case, our current work reveals that various strain conditions (sign, magnitude, and type of strain) and cluster orientations complicate identification of the most favorable configuration for an arbitrary cluster size.

1. Biaxial strain

The plot in Fig. 6 presents a comparison of FC and PHR-type vacancy cluster ($3\leq n\leq 5$) formation-energy curves under biaxial strain. The FC structures are the ground-state configurations of Fig. 2, while the PHR-type configurations are introduced in the upper panel of Fig. 6. As previously described,[14] V_5^{PHR} is actually an FC configuration proposed by Makhov and Lewis,[4] but is 0.33 eV less favorable than the strain-free, ground-state FC V_5 structure. Since V_5^{PHR} is created through geometrical relaxation of a conventional partial ring structure ($n=5$), we will designate this structure as V_5^{PHR} throughout our discussion.

For each cluster size, it is evident that the ground-state FC structure is energetically more favorable than its corresponding PHR counterpart in the strain-free case. However, for large magnitudes of tensile biaxial strain ($\varepsilon\geq 2$), we observe that both V_3^{PHR} and V_5^{PHR} become more favorable than V_3 and V_5, respectively. This same behavior might also occur for the tetravacancy case, but the large difference in strain-free formation energies per vacancy [$\hat{E}_f(4,0\%)=1.86$ eV (V_4) and $\hat{E}_f(4,0\%)=2.20$ eV (V_4^{PHR})] prohibits V_4^{PHR} favorability in the range of strain investigated. From the formation-energy curves in Fig. 6, it is apparent that the potential favorability of the PHR configurations in each case is made possible by the prominent flatness in the $\hat{E}_f(n,\varepsilon)$ curves under tensile strain. The flatness is much more apparent for structures with incomplete fourfold coordination, as for V_3^{PHR} and V_4^{PHR}, rather than the mild reduction in slope exhibited for V_5^{PHR} (FC). This observation is further supported upon review of Fig. 4(b) which shows a flat response under tensile strain for V_2^{PHR}, but only a subtle reduction in slope for the limiting PHR case of FC V_6.

2. Uniaxial strain

Motivated by the orientation effect observed under uniaxial strain [Fig. 4(a)] for both V_2 and V_6, we proceeded to investigate other PHR-type clusters to confirm generality of this behavior. Figure 7 presents $\hat{E}_f(n,\varepsilon)$ curves as a function of uniaxial strain for both FC and PHR-type vacancy clusters in the size range $n=2-6$. It is evident from our results that the A orientation of PHR-type defects is less sensitive to uniaxial strain than the C orientation. At a first glance, the trivacancy case appears to offer the only exception; however, further inspection of the ring vacancy configuration in the upper panel of Fig. 7 reveals that $V_3^{\mathrm{A,PHR}}$ and $V_3^{\mathrm{C,PHR}}$ are identical with respect to uniaxial strain. The C orientation of the ring structure in Fig. 7 shows that there are two unique bonding arrangements with respect to strain: (1) bonds 2-3 and 5-6 and (2) bonds 1-2, 1-6, 3-4, and 4-5. V_3^{PHR} is formed by removal of the atoms delimiting bonds 1-2 and 2-3, so V_3^{PHR} has one bond from each unique bond set. Therefore, conversion of $V_3^{\mathrm{A,PHR}}$ to $V_3^{\mathrm{C,PHR}}$ is irrelevant with respect to strain because there is still one bond representing each bonding set after reorientation. For all other PHR configurations in Fig. 7, the orientation change between A and C augments the bond count between the two bonding groups and an orientation effect is observed in the $\hat{E}_f(n,\varepsilon)$ data. The behavior of the strain-free, ground-state FC configurations ($3\leq n\leq 5$) are also provided in both orientations for comparison. $V_5^{\mathrm{A,PHR}}$ under high tension provides the only case in our data where a PHR structure is predicted to be more stable ($\varepsilon\geq 3\%$) than the corresponding strain-free, ground-state FC structure.

Another important aspect of our results is the data omitted in Fig. 7(c) for the $V_4^{\mathrm{C,PHR}}$ $\hat{E}_f(4,\varepsilon)$ curve. In this case, we found sufficient tensile strain ($\varepsilon>1\%$) initiated configuration changes, so this data is not shown for the sake of clarity.

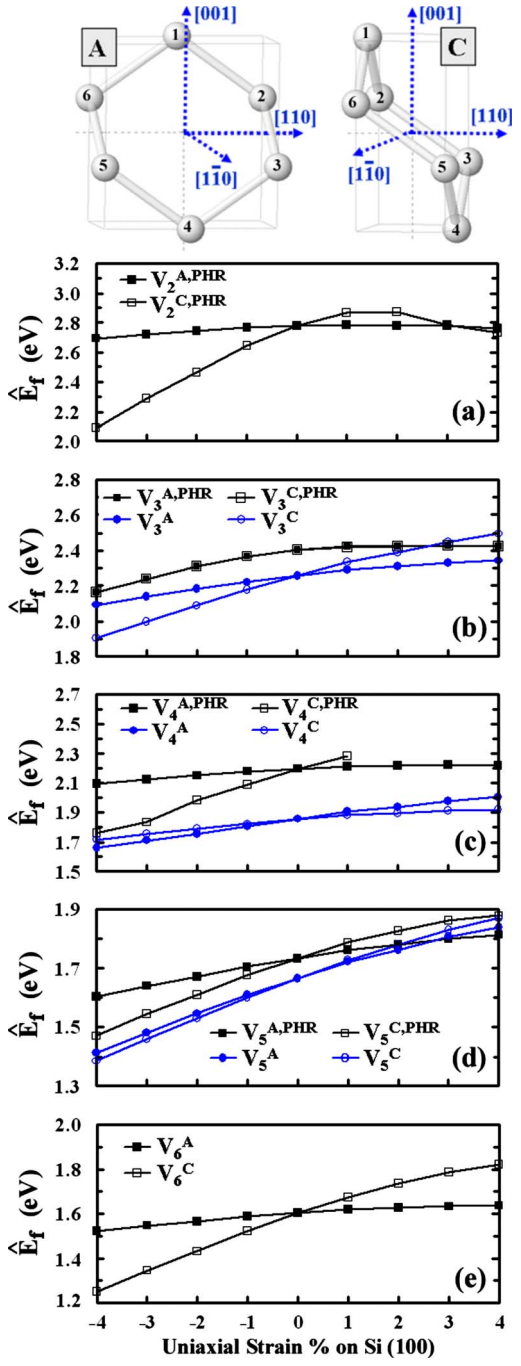

FIG. 7. (Color online) Formation energy per vacancy as a function of uniaxial strain applied along [110] for each cluster size ($2 \leq n \leq 6$) for both FC and PHR configurations in both A and C orientations, as applicable. Square markers (black) represent PHR-type configurations while circular markers (blue) represent FC configurations, where applicable. Solid markers represent A orientations, while open markers represent C orientations. The upper panel is a visual aid for orientation of the general six-membered ring with respect to the Si lattice. The vacancy sites are numbered to facilitate discussion in the order in which atoms were removed to form PHR-type ring defects. In orientation A, applied strain along [110] is parallel to an imaginary surface formed by the missing constituents of the ring. In orientation C, the applied strain direction is rotated 90° about [001] and is orthogonal to these missing bonds: 1-2, 1-6, 3-4, and 4-5.

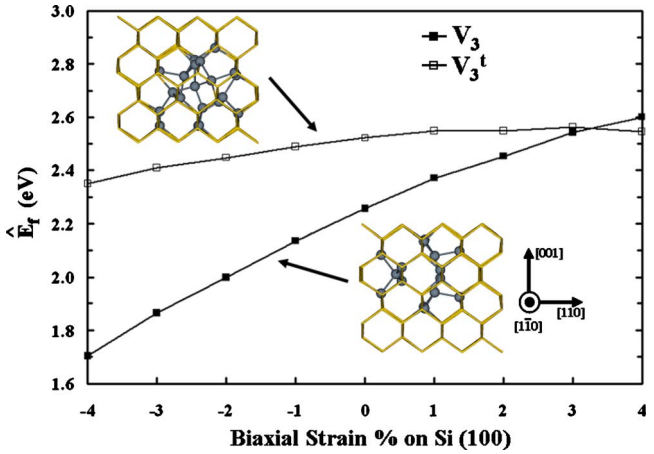

FIG. 8. (Color online) Formation energy per vacancy as a function of biaxial strain for the strain-free, ground-state FC V_3 structure and a FC trivacancy configuration (V_3^t) identified by formation under tensile biaxial strain conditions. Inset cluster configurations are shown along [1$\bar{1}$0]. Light gray (gold) wireframe represents bulk crystalline Si. Dark gray spheres represent highly strained atoms neighboring the vacancy clusters.

Application of both 2% and 3% uniaxial strain to the strain-free configuration of $V_4^{C,PHR}$ generated unoptimized configurations with the same bond topologies as the strain-free, ground-state FC V_4^C structure. This observation is significant since it suggests that strain can enable interconversion between PHR-type and FC vacancy structures. Finally, application of 4% uniaxial strain to the strain-free configuration of $V_4^{C,PHR}$ generated a different configuration deficient of complete fourfold coordination that is distinct from either the V_4 or V_4^{PHR} configurations.

C. Configuration changes

As previously described, strain can initiate configuration changes in vacancy clusters, just as our previous work[26,27] described both structural distortions and configuration changes for interstitial clusters in strained Si. To further our study, we used the integrated atomic modeling procedure[14–18] to generate vacancy-cluster configurations under both 3% compressive and 3% tensile biaxial strain conditions for cluster sizes up to $n=12$. For the sake of brevity, we only describe the highlights from our comparison of clusters formed strain-free to those formed under strain and reserve the details to be published elsewhere. Overall, the vacancy clusters formed under tensile conditions provided more interesting results, particularly in terms of formation energy responses as a function of strain.

In Fig. 8, we provide $\hat{E}_f(3,\varepsilon)$ behavior as a function of strain for both the strain-free, ground-state FC V_3 configuration and a trivacancy structure (V_3^t), also with fourfold coordination, formed under 3% tensile biaxial strain. The formation energies are nearly degenerate at 3% tensile strain [$\hat{E}_f(3,3\%)=2.54$ eV (V_3) and $\hat{E}_f(3,3\%)=2.56$ eV (V_3^t)], so the preferred structure observed at these conditions is subject to variation with modeling parameters, such as initial va-

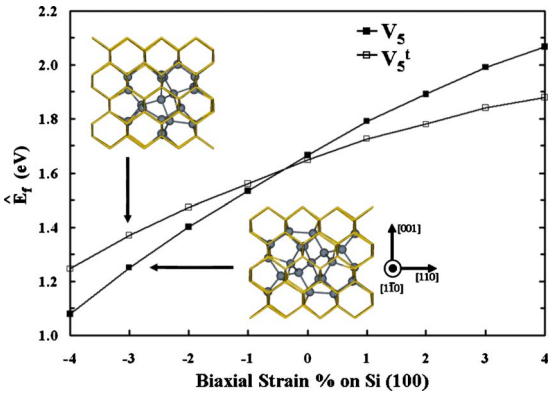

FIG. 9. (Color online) Formation energy per vacancy as a function of biaxial strain for the strain-free, ground-state FC V_5 structure and a FC pentavacancy configuration (V_5^t) identified by formation under tensile biaxial strain conditions. These structures are approximately degenerate under strain-free conditions. Inset cluster configurations are shown along [1$\bar{1}$0]. Light gray (gold) wireframe represents bulk crystalline Si. Dark gray spheres represent highly strained atoms neighboring the vacancy clusters.

cancy seeding in the MMC stage. While V_3 is relatively more stabilized under compressive conditions, V_3^t becomes favored under high tension ($\varepsilon > 3\%$).

In Fig. 9, we similarly provide $\hat{E}_f(5,\varepsilon)$ behavior as a function of strain for both the strain-free, ground-state FC V_5 configuration and a pentavacancy structure (V_5^t), also with fourfold coordination, formed under 3% tensile biaxial strain. In this case, formation energies are nearly degenerate under strain-free conditions [$\hat{E}_f(5,0\%)=1.67$ eV (V_5) and $\hat{E}_f(5,0\%)=1.65$ eV (V_5^t)]. As additional qualification of the approximate degeneracy of these structures, we note that Ref. 14 generated V_5 as the ground-state configuration, while our previous work (Ref. 15) generated V_5^t through annealing of $V_4+V \rightarrow V_5$ during TBMD simulations at 1400 K. Our results indicate that the stability of V_5^t is less sensitive to strain than V_5 and that V_5^t is the preferred orientation under tensile conditions.

IV. SUMMARY

The effect of strain on the stability and structure of small, neutral Si vacancy clusters (V_n, $n \leq 12$) was investigated using periodic DFT calculations. Our results indicate that compressive strain generally stabilizes vacancy clusters, which is complementary to the conclusions of our previous work[25–27] that showed that tensile strain stabilizes Si interstitial clusters. The magnitude of stabilization provided by biaxial compression is generally greater than the magnitude of stabilization observed under uniaxial compression.

Similar to our previous work on interstitials, we also observe orientation effects for vacancy clusters in uniform strain fields. The C_{2h}-symmetry configurations of V_4 and V_8 exhibit orientation-dependent behavior under biaxial strain in correlation with the orientation-dependent behavior shown by interstitial clusters with C_{2h} symmetry. This observation is significant because it emphasizes the critical role that cluster symmetry performs in orientation-dependent stabilization in strained Si, regardless of cluster composition.

Our calculations show that strain conditions can modulate the relative stability of competing FC and PHR-type configurations. While FC configurations are more favorable for small vacancy clusters in strain-free environments, PHR-type configurations become preferred under certain tensile conditions in both biaxial and uniaxial cases. The relative stabilization of PHR-type configurations under tension is largely attributable to the flat nature of the formation-energy dependence on strain that is generally exhibited by clusters with incomplete fourfold coordination. In addition, our results illuminate a general orientation effect for PHR-type configurations ($2 \leq n \leq 6$) under uniaxial strain related to alignment of the parent ring structure with respect to the direction of applied strain.

Our simulations also demonstrate that strain of sufficient magnitude can initiate configuration changes. We provide two examples (V_3^t and V_5^t) of vacancy configurations we identified by cluster formation under 3% tensile biaxial strain. These particular structures were highlighted because they exhibited different formation-energy responses as a function of strain when compared to their counterpart configurations formed under strain-free conditions. Our study furthers the understanding of Si vacancy clusters by providing insight into the influence that strain has on the stability and structure of vacancy defects, which is an important step toward property prediction and ultimately defect engineering in Si-based materials.

ACKNOWLEDGMENTS

We acknowledge National Science Foundation (Grant No. CBET-0933557) and Robert A. Welch Foundation (Grant No. F-1535) for their financial support. S. Lee is grateful for support from the Donald D. Harrington Graduate Fellows Program. We would also like to thank the Texas Advanced Computing Center for use of their computing resources.

*Author to whom correspondence should be addressed; gshwang@che.utexas.edu

[1] D. A. Abdulmalik and P. G. Coleman, Phys. Rev. Lett. **100**, 095503 (2008).
[2] A. La Magna, S. Coffa, and L. Colombo, Phys. Rev. Lett. **82**, 1720 (1999).
[3] E. Dornberger, D. Temmler, and W. Von Ammon, J. Electrochem. Soc. **149**, G226 (2002).
[4] D. V. Makhov and L. J. Lewis, Phys. Rev. Lett. **92**, 255504 (2004).
[5] S. K. Estreicher, Phys. Status Solidi B **217**, 513 (2000).
[6] J. L. Hastings, S. K. Estreicher, and P. A. Fedders, Phys. Rev. B

56, 10215 (1997).
[7] T. E. M. Staab, A. Sieck, M. Haugk, M. J. Puska, Th. Frauenheim, and H. S. Leipner, Phys. Rev. B **65**, 115210 (2002).
[8] J. S. Williams, M. J. Conway, B. C. Williams, and J. Wong-Leung, Appl. Phys. Lett. **78**, 2867 (2001).
[9] G. S. Hwang and W. A. Goddard III, Phys. Rev. B **65**, 233205 (2002).
[10] D. J. Chadi and K. J. Chang, Phys. Rev. B **38**, 1523 (1988).
[11] M. G. Ganchenkova, S. Nicolaysen, V. A. Borodin, E. Halvorsen, and R. M. Nieminen, Mater. Sci. Eng. B **134**, 244 (2006).
[12] A. Bongiorno and L. Colombo, Phys. Rev. B **57**, 8767 (1998).
[13] A. Zywietz, J. Furthmuller, and F. Bechstedt, Phys. Status Solidi B **210**, 13 (1998).
[14] S. Lee and G. S. Hwang, Phys. Rev. B **78**, 125310 (2008).
[15] S. Lee, R. J. Bondi, and G. S. Hwang, Phys. Rev. B **80**, 245209 (2009).
[16] S. Lee and G. S. Hwang, Phys. Rev. B **77**, 085210 (2008).
[17] S. Lee and G. S. Hwang, Phys. Rev. B **78**, 045204 (2008).
[18] S. Lee, R. J. Bondi, and G. S. Hwang, Mol. Simul. **35**, 867 (2009).
[19] S. E. Thompson, G. Sun, Y.-S. Choi, and T. Nishida, IEEE Trans. Electron Devices **53**, 1010 (2006).
[20] K. Derbyshire, Solid State Technol. **50**, 38 (2007).
[21] J. P. Perdew and Y. Wang, Phys. Rev. B **45**, 13244 (1992).
[22] G. Kresse and J. Hafner, Phys. Rev. B **47**, 558 (1993); **49**, 14251 (1994); G. Kresse and J. Furthmuller, Comput. Mater. Sci. **6**, 15 (1996); Phys. Rev. B **54**, 11169 (1996).
[23] G. Kresse and J. Furthmuller, *VASP the Guide* (Vienna University of Technology, Vienna, 2001).
[24] D. Vanderbilt, Phys. Rev. B **41**, 7892 (1990).
[25] R. J. Bondi, S. Lee, and G. S. Hwang, Phys. Rev. B **79**, 104106 (2009).
[26] R. J. Bondi, S. Lee, and G. S. Hwang, Appl. Phys. Lett. **94**, 264101 (2009).
[27] R. J. Bondi, S. Lee, and G. S. Hwang, Phys. Rev. B **80**, 125202 (2009).
[28] J. Singh, *Physics of Semiconductors and Their Heterostructures* (McGraw-Hill, New York, 1993).
[29] L. Lin, T. Kirichenko, B. R. Sahu, G. S. Hwang, and S. K. Banerjee, Phys. Rev. B **72**, 205206 (2005).
[30] P. Bhattacharya, *Semiconductor Optoelectronic Devices* (Prentice Hall, Upper Saddle River, NJ, 1997).
[31] C. G. Van de Walle and R. M. Martin, Phys. Rev. B **34**, 5621 (1986).
[32] M. E. Levinshtein, S. L. Rumyantsev, and M. S. Shur, *Handbook Series on Semiconductor Parameters* (World Scientific, London, 1996), Vol. 1, p. 29.